Reaction of Alkynes with $Rh_4(CO)_{12}$. A Mid-Infrared Vibrational and Kinetic Study of (μ_4-η^2-alkyne)$Rh_4(CO)_8(\mu$-$CO)_2$

Ayman D. Allian, Martin Tjahjono, and Marc Garland*

Department of Chemical and Biomolecular Engineering, 4 Engineering Drive 4, National University of Singapore, Singapore 117576

Received November 21, 2005

The pure component mid-infrared spectra of the butterfly clusters (μ_4-η^2-alkyne)$Rh_4(CO)_8(\mu$-$CO)_2$, alkyne = 3-hexyne, 1-heptyne, 1-octyne, 4-octyne, 1-phenyl-1-hexyne, and 1-phenyl-1-butyne, were obtained from multicomponent solutions using band-target entropy minimization (BTEM). DFT was used to carry out full geometric optimization and mid-infrared vibrational prediction of (μ_4-η^2-2-butyne)$Rh_4(CO)_8(\mu$-$CO)_2$ and (μ_4-η^2-propyne)$Rh_4(CO)_8(\mu$-$CO)_2$ as simple models for the terminal and symmetric alkyne clusters, respectively. The predicted spectra were in good agreement with the experimentally obtained deconvoluted pure component spectra of this class of complexes. The kinetics for the formation of the butterfly cluster (μ_4-η^2-3-hexyne)$Rh_4(CO)_8(\mu$-$CO)_2$ from the reaction of $Rh_4(CO)_{12}$ with 3-hexyne in *n*-hexane, i.e., $Rh_4(CO)_{12}$ + 3-hexyne → (μ_4-η^2-3-hexyne)$Rh_4(CO)_8(\mu$-$CO)_2$ + 2CO, was also investigated. The rate of formation of the butterfly cluster was found to follow the rate expression, rate = $k_{obs}[Rh_4(CO)_{12}]^1[3\text{-hexyne}]^1[CO]^{-1}$, with the apparent activation parameters $\Delta H^{\ddagger} = 123.6 \pm 11.0$ kJ/mol·K and $\Delta S^{\ddagger} = (7 \pm 4) \times 10$ J·mol^{-1}·K^{-1}. A mechanism is proposed consistent with the observed kinetic rate expression. This involves a dissociation of one of the carbonyl ligands from $Rh_4(CO)_{12}$ prior to the alkyne coordination.

Introduction

The reaction of alkynes with organometallic clusters has been a subject of considerable experimental as well as theoretical interest due to the wide variety of coordination modes possible.[1−3] Thus the coordination of alkynes to organometallic clusters of various nuclearities has attracted considerable attention. In particular, the decrease in bond order of the coordinated alkynes, and hence lengthening of the carbon−carbon bond, due to the back-bonding from multiple metal centers has been an issue of keen interest. Such studies have also provided an excellent model for the understanding of the adsorption/coordination of alkynes to metal surfaces.[2−4]

In addition to the interest in alkynes and metal clusters due to their coordination chemistry alone, the synthetic utility of stoichiometric metal-mediated and catalytic reactions involving alkynes has been the focus of numerous other studies. For example, in the absence of other reactants, alkyne trimerization has been observed using a wide variety of metals such as $CpCo(CO)_2$.[5] Alkynes are also known to react with a second reagent, i.e., alkenes, to give conjugated dienes.[6]

Perhaps most notably, alkynes react with both alkenes and CO to give substituted cyclopentenones. The Pauson−Khand[7,8] reaction has been shown to occur as both a stoichiometric metal-mediated and catalytic reaction.[9] Both intramolecular and intermolecular Pauson−Khand reactions are used as the main routes to generate high-value-added and biologically active substituted cyclopentenones. Substituted cyclopentenones are of considerable interest to the pharmaceutical industry, as they often display high potency as antitumor and antibacterial agents.[10]

The rhodium carbonyl cluster $Rh_4(CO)_9(\mu$-$CO)_3$, first prepared and characterized by Chini,[11−13] has often been the group 9 cluster of choice for mechanistic and synthetic studies involving tetranuclear clusters.[14−17] Recent reports indicate that $Rh_4(CO)_{12}$[18] and other rhodium-based organometallics[19] can mediate the Pauson−Khand reaction, even catalytically. However, understanding of the coordination chemistry of $Rh_4(CO)_{12}$ with alkynes is minimal. Diphenylacetylene was reported to react with $Rh_4(CO)_{12}$, and the new species was tentatively assigned to be (μ_4-η^2-$C_6H_5C{\equiv}CC_6H_5$)$Rh_4(CO)_8(\mu$-$CO)_2$[20] based on its mid-infrared spectral similarity to the butterfly cluster (μ_4-η^2-

* To whom correspondence should be addressed. E-mail: chemvg@nus.edu.sg. Phone: +65-6-874-6617. Fax: +65-6-779-1936.

(1) Jeannin, Y. *Transition Met. Chem.* **1993**, *18*, 122.
(2) Muetterties, E. L. *Science* **1977**, *196*, 839.
(3) Stanghellini, P. L.; Rossetti, R. *Inorg. Chem.* **1990**, *29*, 2047.
(4) Kesmodel, L. L.; Baetzold, R. C.; Somorjai, G. A. *Surf. Sci.* **1977**, *66*, 299.
(5) Sünkel, K. *J. Organomet. Chem.* **1990**, *391*, 247.
(6) See for example: (a) Trost, B. M.; Machacek, M.; Schnaderbeck, M. J. *Org. Lett.* **2000**, *2*, 1761. (b) Herrmann, W. A.; Fischer, R. A.; Herdtweck, E. *Organometallics* **1989**, *8*, 2821.
(7) Khand, I. U.; Knox, G. R.; Pauson, P. L.; Watts, W. E. *J. Chem. Soc., Chem. Commun.* **1971**, 36.
(8) Khand I. U.; Knox, G. R.; Pauson, P. L.; Watts, W. E. *J. Chem. Soc., Perkin Trans. 1* **1973**, 975.
(9) See for example: (a) Gibson, S. E.; Stevenazzi, A. *Angew. Chem., Int. Ed.* **2003**, *42*, 1800. (b) Blanco-Urgoiti, J.; Perez-Castells, J. *Chem. Soc. Rev.* **2004**, *33*, 32. (c) Brummond, K. M.; Joseph, J. L. *Tetrahedron* **2000**, *56*, 3263. (d) Gibson, S. E.; Mainolfi, N. *Angew. Chem., Int. Ed.* **2005**, *44*, 3022.
(10) Gibson, S. E.; Lewis, S. E.; Mainolfi, N. *J. Organomet. Chem.* **2004**, *689*, 3873.
(11) Chini, P.; Martinengo, S. *Chem. Commun.* **1968**, *5*, 251.
(12) Chini, P.; Martinengo, S. *Inorg. Chim. Acta* **1969**, *3*, 315.
(13) Chini, P.; Heaton, B. T. *Top. Curr. Chem.* **1977**, *71*, 1.
(14) Cotton, F. A.; Kruczynski, L.; Lewis, J.; Shapiro, B. L.; Johnson, L. F. *J. Am. Chem. Soc.* **1972**, *94*, 6191.
(15) Evans, J.; Johnson, B. F. G.; Lewis, J.; Norton, J. R.; Cotton, F. A. *J. Chem. Soc., Chem. Commun.* **1973**, *21*, 807.
(16) Band, E.; Muetterties, E. L. *Chem. Rev.* **1978**, *78*, 8, 636.
(17) Roberts, Y. V.; Johnson, B. F.; Benfield, R. E. *Inorg. Chim. Acta* **1995**, *229*, 221.
(18) Kobayashi, T.; Koga, Y.; Naraska, K. *J. Organomet. Chem.* **2001**, *624*, 73.

10.1021/om0510019 CCC: $33.50
Publication on Web 03/21/2006

CH≡CH)$Co_4(CO)_8(\mu\text{-}CO)_2$.[21] Stanghellini[22] later carried out a detailed study of (μ_4-η^2-CH≡CH)$Co_4(CO)_8(\mu\text{-}CO)_2$ where both the mid-infrared assignment and the X-ray structure were reported. Shortly thereafter, Horvath[23] reported the X-ray single-crystal structure of the mixed metal butterfly cluster (μ_4-η^2-RC_2R)$Co_2Rh_2(CO)_8(\mu\text{-}CO)_2$, alkyne = C_6F_5, Ph. In addition, the X-ray single-crystal structure[24] of (μ_4-η^2-PhC_2Ph)$Co_3Rh(CO)_8(\mu\text{-}CO)_2$ and recently the structure of (μ-dmad)$_3CoRh_3(CO)_9$, dmad = $(CH_3O)COCCCO(OCH_3)$, were reported.[25]

In the present contribution, understanding of the reactivity and coordination chemistry of alkynes with $Rh_4(CO)_{12}$ is considerably extended. The pure component mid-infrared spectra of various butterfly clusters formed by reacting $Rh_4(CO)_{12}$ with symmetric, terminal, asymmetric alkynes were obtained. DFT calculations were performed on (μ_4-η^2-2-butyne)$Rh_4(CO)_8(\mu\text{-}CO)_2$ and (μ_4-η^2-propyne)$Rh_4(CO)_8(\mu\text{-}CO)_2$ as simple models for the symmetric and terminal alkyne clusters. The DFT-optimized geometries yielded predicted infrared spectra that were very consistent with the experimentally observed spectra. The DFT-optimized geometries for the butterfly clusters are reported. The kinetics of the reaction of $Rh_4(CO)_{12}$ with 3-hexyne in *n*-hexane solutions was also investigated in detail using in-situ infrared spectroscopy.

Results and Discussion

High-Resolution Vibrational Study of (μ_4-η^2-3-hexyne)$Rh_4(CO)_8(\mu\text{-}CO)_2$. The reaction of 40 mg of $Rh_4(CO)_{12}$ with 0.95 equiv of 3-hexyne under atmospheric argon, in 100 mL of *n*-hexane as a solvent, was monitored via in-situ FTIR spectroscopy using 1 cm^{-1} resolution. The collected reaction spectra were deconvoluted using band target entropy minimization (BTEM).[26,27] Besides the pure component spectra of the starting materials, $Rh_4(CO)_9(\mu\text{-}CO)_3$ and 3-hexyne, a new mid-infrared spectrum was obtained, Figure 1c. The band positions and intensity are strikingly similar to the infrared spectrum of the species reported to be (μ_4-η^2-PhC_2Ph)$Rh_4(CO)_8(\mu\text{-}CO)_2$[20] and species ($\mu_4$-$\eta^2$-$HC_2H$)$Co_4(CO)_8(\mu\text{-}CO)_2$, which was confirmed by X-ray.[22]

Density functional theory (DFT) was used to carry out full geometric optimization and mid-infrared vibrational prediction of the slightly simpler species (μ_4-η^2-2-butyne) $Rh_4(CO)_8(\mu\text{-}CO)_2$ (see Experimental Section for further details). Figure 1 shows that the experimental spectrum and the DFT-predicted spectrum are in good agreement. The vibrational patterns are similar, and the relative intensities of the bands are similar. The overlap of two vibrational modes in the experimental spectrum at 2027 and 2036 cm^{-1} is clearly predicted by DFT at 1998 and 2006 cm^{-1}.

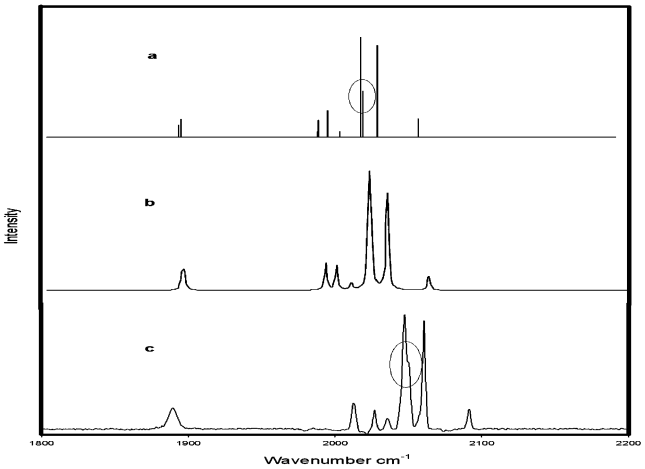

Figure 1. DFT-predicted spectrum of (μ_4-η^2-2-butyne)$Rh_4(CO)_8(\mu\text{-}CO)_2$ using (a) GaussView03 and (b) Molden43 and the (c) high-resolution experimental spectrum of (μ_4-η^2-3-hexyne)$Rh_4(CO)_8(\mu\text{-}CO)_2$.

Table 1 indicates that the current density functional method overestimated the wavenumber of the bridging carbonyls in (μ_4-η^2-symmetric alkyne)$Rh_4(CO)_8(\mu\text{-}CO)_2$ by ca. 0.3% while underestimating the wavenumber of the terminal metal carbonyl by ca. 1.3%. The DFT and experimental wavenumbers for (μ_4-η^2-symmetric alkyne)$Rh_4(CO)_8(\mu\text{-}CO)_2$ are compared to the complex (μ_4-η^2-PhC_2Ph)$Rh_4(CO)_8(\mu\text{-}CO)_2$ reported by Iwashita and Tamura[20] and the complex (μ_4-η^2-HC_2H)$Co_4(CO)_8(\mu\text{-}CO)_2$ reported by Stangellini.[22]

The optimized structure of (μ_4-η^2-2-butyne) $Rh_4(CO)_8(\mu\text{-}CO)_2$ is shown in Figure 2. The rhodium skeleton appears as a butterfly with Rh(3) and Rh(4) occupying the wingtip positions and Rh(1) and Rh (2) forming the body. There are two inequivalent bridging carbonyls and eight terminal carbonyls. The alkyne group, C(6)−C(7), is not exactly parallel to the Rh(1)−Rh(2) bond, in agreement with the reported X-ray of (μ_4-η^2-HC_2H)$Co_4(CO)_8(\mu\text{-}CO)_2$[22] and ($\mu_4$-$\eta^2$-$RC_2H$)$Co_2Rh_2(CO)_6(\mu\text{-}CO)_4$, R = $FeCp_2$.[28] The structure has low symmetry (approximate C_2 symmetry). The Rh(2)−Rh(3) predicted bond length is 2.81 Å, while the Rh(2)−Rh(4) is 2.71 Å. The predicted dihedral angle between the M(1)−M(2)−M(3) and M(1)−M(4)−M(3) planes is 120.8°, consistent with the reported experimental values of 116° for (μ_4-η^2-HC_2H)$Co_4(CO)_8(\mu\text{-}CO)_2$[22] and 116.9° for ($\mu_4$-$\eta^2$-$RC_2R$)$Co_2Rh_2(CO)_8(\mu\text{-}CO)_2$, R = C_6F_5.[23] It should be mentioned that in the two reported mixed Co_2Rh_2 alkyne clusters, two CO ligands are semibridged, whereas in neither the X-ray structure of (μ_4-η^2-HC_2H)$Co_4(CO)_8(\mu\text{-}CO)_2$ nor the DFT-predicted geometry of (μ_4-η^2-symmetric alkyne)$Rh_4(CO)_8(\mu\text{-}CO)_2$ are there indications for semibridged behavior.

The coordinated alkyne in Figure 2 is predicted to have a bond length of ca. 1.42 Å, and the bond angle C17−C6−C7 is 124°. The reported bond lengths for the alkyne moieties in refs 22, 23, 24, and 28 were 1.399, 1.369, 1.42, and 1.419 Å, respectively. These values can be compared to a bond length of 1.22 Å predicted for free 2-butyne using the same DFT method, PBE/DGDZVP. Overall, the coordinated alkyne in Figure 2 has a ca. 1.5 bond order.[2]

(19) See for example: (a) Schmid, T. M.; Consiglio, G. *Chem. Commun.* **2004**, *20*, 2318. (b) Jeong, N.; Sung, B. K.; Choi, Y. K. *J. Am. Chem. Soc.* **2000**, *122*, 6771. (c) Shibata, T.; Toshida, N.; Takagi, K. *Org. Lett.* **2002**, *4*, 1619. (d) Suh, W. H.; Choi, M.; Lee, S. I.; Chung, Y. K. *Synthesis* **2003**, 2169. (e) Jeong, N.; Lee, S.; Byung, B. K. *Organometallics* **1998**, *17*, 3642. (f) Koga, Y.; Kobayashi, T.; Narasaka, K. *Chem. Lett.* **1998**, 249. (g) Kobayashi, P. T.; Koga, Y.; Naraska, K. *J. Organomet. Chem.* **2001**, *624*, 73. (h) Jeong, N.; Sung, B. K.; Kim, J. S.; Park, S. B.; Seo, S. D.; Shin, J. Y.; In, K. Y.; Choi, Y. K. *Pure Appl. Chem.* **2002**, *74*, 85.

(20) Iwashita, Y.; Tamura, F. *Bull. Chem. Soc. Jpn.* **1970**, *43*, 1517.

(21) Kruerk, U.; Hubel, W. *Chem. Ber.* **1961**, *95*, 2829.

(22) Gervasio, G.; Rossetti, R.; Stanghellini, P. L. *Organometallics* **1985**, *4*, 1612.

(23) Horvath, I. T.; Zsolnai, L.; Huttner, G. *Organometallics* **1986**, *5*, 180.

(24) Tunik, S. P.; Krym, V. R.; Starova, G. L.; Nikol'skii, A. B.; Podkorytov, I. S.; Ooi, S.; Yamasaki, M.; Shiro, M. *J. Organomet. Chem.* **1997**, *481*, 83.

(25) Watson, W. H.; Poola, B.; Richmond, M. G. *Organometallics* **2005**, *24*, 4687.

(26) Chew, W.; Widjaja, E.; Garland, M. *Organometallics* **2002**, *21*, 1882.

(27) Widjaja, E.; Li, C.; Garland, M. *Organometallics* **2002**, *21*, 1991.

(28) Zhu, B.; Zhang, W.; Zhao, Q.; Bian, Z.; Hu, B.; Zhang, Y.; Yu-Hua, Y.; Sun, J. *J. Organomet. Chem.* **2002**, *650*, 181.

Table 1. Mid-infrared Carbonyl Vibrational Spectra (cm^{-1}) of (μ_4-η^2-symmetric alkyne)$M_4(CO)_8(\mu$-$CO)_2$ Butterfly Clusters (M = Rh, Co)

	bridging		terminal							
DFT[a]	1893	1895	1990	1991	1998	2006	2021	2023	2033	2061
3-hexyne[a]	1889		2012.6		2027	2036	2047	2050	2061	2091
PhC_2Ph[b]	1885		2020		2035		2055		2070	2095
acetylene[c]	1879		2000		2023		2040	2043	2053	2093

[a] This study M = Rh. [b] Ref 20 M = Rh. [c] Ref 22 M = Co.

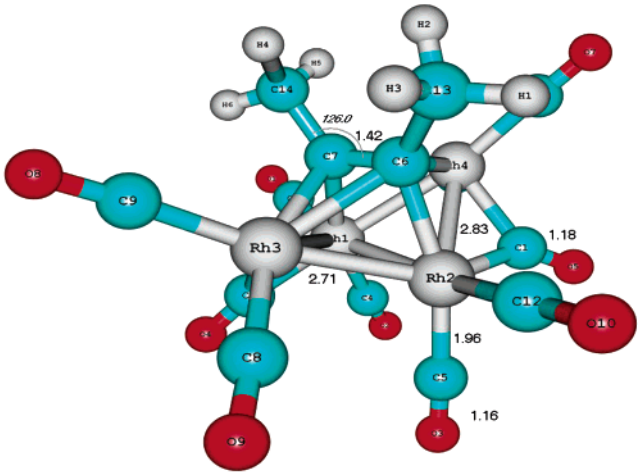

Figure 2. DFT-optimized geometry of (μ_4-η^2-2-butyne)$Rh_4(CO)_8$-(μ-$CO)_2$ using PBE/DGDZVP.

Low-Resolution Vibrational Study of (μ_4-η^2-terminal alkyne)$Rh_4(CO)_8(\mu$-$CO)_2$]. Using a similar approach, the reaction of 40 mg of $Rh_4(CO)_{12}$ with 0.95 equiv of terminal alkynes, namely, 1-heptyne or phenylacetylene, was monitored via in-situ mid-infrared FTIR spectroscopy using 4 cm^{-1} resolution. The collected reaction spectra were deconvoluted using BTEM. Again, new pure component spectra were obtained. These are shown in Figure 3c,d along with the vibrational predictions, Figure 3a,b, obtained for full geometrically optimization of (μ_4-η^2-propyne)$Rh_4(CO)_8(\mu$-$CO)_2$.

Figure 3 shows that the DFT-predicted spectrum of (μ_4-η^2-propyne)$Rh_4(CO)_8(\mu$-$CO)_2$ is in very good agreement with experimentally observed deconvoluted spectra of (μ_4-η^2-1-heptyne)$Rh_4(CO)_8(\mu$-$CO)_2$ and (μ_4-η^2-phenylacetylene)Rh_4-$(CO)_8(\mu$-$CO)_2$. A more detailed comparison of the vibrational spectra is provided in Table 2. The mid-infrared spectra of the class (μ_4-η^2-terminal alkyne)$Rh_4(CO)_8(\mu$-$CO)_2$ are slightly but noticeably distinct from those of the class (μ_4-η^2-symmetric alkyne) $Rh_4(CO)_8(\mu$-$CO)_2$.

The DFT-optimized structure of (μ_4-η^2-propyne)$Rh_4(CO)_8$-(μ-$CO)_2$ is shown in Figure 4. Overall, the structural parameters are very close to those observed for the optimized structure of (μ_4-η^2-2-butyne)$Rh_4(CO)_8(\mu$-$CO)_2$.

Low-Resolution Vibrational Study of (μ_4-η^2-asymmetric alkyne)$Rh_4(CO)_8(\mu$-$CO)_2$. For completeness, the reactions of 40 mg of $Rh_4(CO)_9(\mu$-$CO)_3$ with 0.95 equiv each of 1-phenyl-1-butyne and 1-pheny-1-hexyne were monitored using in-situ mid-infrared FTIR spectroscopy using 4 cm^{-1} resolution. The collected data were deconvoluted with BTEM, and again a spectrum with a pattern similar to that observed earlier for terminal and symmetric alkynes was observed. In addition, the length of the aliphatic chain had little or no influence on the observed band positions at 2092, 2064, 2048, 2028, 2013, and 1891 cm^{-1}.

Kinetics. Reaction of the $Rh_4(CO)_9(\mu$-$CO)_3$ with 3-Hexyne. The typical reaction times for symmetric alkynes with $Rh_4(CO)_{12}$ were on the order of hours. These reactions were much slower than those for terminal alkynes with $Rh_4(CO)_{12}$. Therefore, 3-hexyne was selected for kinetic studies of the reaction shown in eq 1. This reaction was studied on the interval of 0−0.95 equiv of alkyne to cluster.

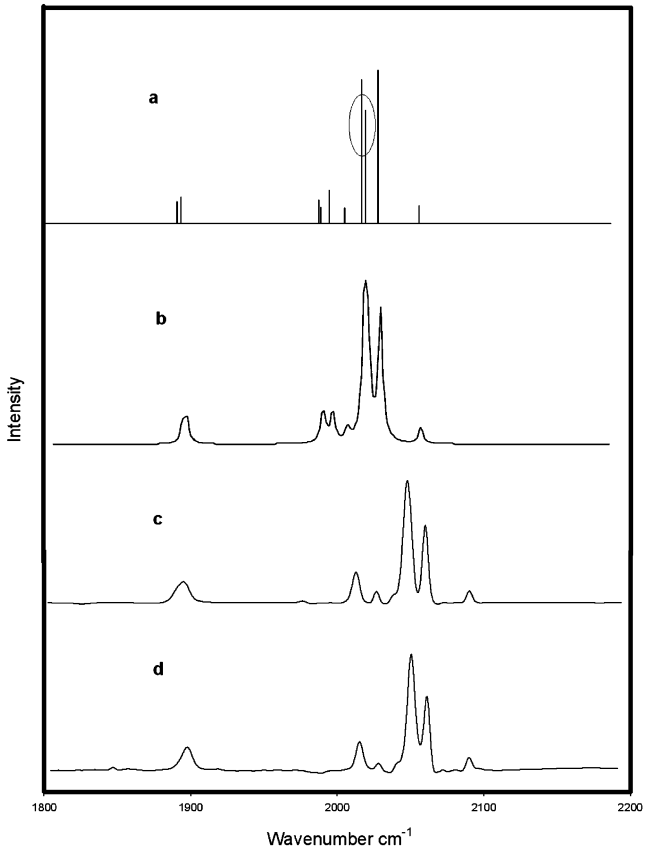

Figure 3. DFT-predicted spectrum of (μ_4-η^2-propyne)$Rh_4(CO)_8$-(μ-$CO)_2$ using (a) GaussView03 and (b) Molden43 and the low-resolution experimental spectra of (c) (1-heptyne)$Rh_4(CO)_8(\mu$-$CO)_2$ and (d) (μ_4-η^2-phenylacetylene)$Rh_4(CO)_8(\mu$-$CO)_2$.

$$Rh_4(CO)_{12} + \text{3-hexyne} \rightarrow (\mu_4\text{-}\eta^2\text{-3-hexyne})Rh_4(CO)_8(\mu\text{-}CO)_2 + 2CO \quad (1)$$

It is rather important to note that the range of this reaction was limited to only 0.95 equiv of alkyne to parent cluster in the present study. Indeed, new very weak signals were observed in the SVD of the present data sets, but these signals were not deconvolutable by BTEM. The presence of these new weak signals suggests other organometallics at very low concentrations. These signals increase significantly in the vicinity of 1 equiv of alkyne to parent cluster, and thus these observations suggest the further fragmentation of the butterfly cluster to binuclear species. A similar observation was made by Horvath[23] for (μ_4-η^2-PhC_2Ph)$Co_2Rh_2(CO)_8(\mu$-$CO)_2$ only after adding

Table 2. Mid-infrared Carbonyl Vibrational Spectra (cm^{-1}) of (μ_4-η^2-terminal alkyne)$Rh_4(CO)_8(\mu\text{-}CO)_2$ Butterfly Clusters

	bridging		terminal							
DFT	1894	1897	1994	1996	2002	2012	2024	2027	2036	2065
1-heptyne	1895		2015		2030	2042	2051		2063	2094
$(Ph)C_2H$	1897		2018		2031	2044	2054		2066	2095

excess alkynes. The nature and the structure of the species in homometallic rhodium experiments will be the subject of further study.

Spectroscopic Aspects. Twelve isothermal batch reactions were conducted under 1 atm of pressure of Ar and/or CO using hexane as a solvent. The concentrations and the operating condition were design to allow mechanistic investigation (see Experimental Section for details). All experiments were monitored via on-line mid-infrared FTIR spectroscopy with a resolution of 4 cm^{-1}.

As an example, the raw spectra of the carbonyl vibration region ν(CO) at 1800−2200 cm^{-1} for batch number 3 are shown in Figure 6. Upon adding 0.95 equiv of 3-hexyne (6 μL), the decline of the $Rh_4(CO)_9(\mu\text{-}CO)_3$ band and the rise of new bands was observed.

Pure Component Spectra. BTEM was used to deconvolute the pure component spectra present. The rhodium organometallics observed are shown in Figure 7. The pure component spectrum of the starting material $Rh_4(CO)_9(\mu\text{-}CO)_3$ at 2073.8, 2069.6, 2043.2, and 1886.4 cm^{-1} was consistent with previous studies and references therein.[29] The vibrational spectrum of (μ_4-η^2-$C_2H_5CCC_2H_5$)$Rh_4(CO)_8(\mu\text{-}CO)_2$ was reconstructed with excellent high signal-to-noise and is in excellent agreement with high-resolution spectra shown in Figure 1. Furthermore, the spectrum of $Rh_6(CO)_{16}$ was observed, with bands at 2075 and 1819.6 cm^{-1}. As $Rh_6(CO)_{16}$ is present at trace levels, its spectra possessed few artifacts and had lower signal-to-noise ratio. The spectrum of the newly identified all-terminal $Rh_4(CO)_{12}$, which is present at only a 1% level, was not deconvolutable.[29] No other organometallic pure component spectra could be reconstructed.

Relative Concentrations. Upon obtaining the pure component spectra, which are not yet scaled to the correct extinction coefficient, their relative concentration profiles (contributions to overall signal) can be readily obtained as shown in Figure 8. These relative concentration profiles are simply the contribution of each pure component signal to the total experimentally measured spectral signal. The relative concentration profiles of the species in batch 3 are shown in Figure 8. The organometallic species contribute ca. 20% of the experimental signal, while the rest of the signal is coming from the background, moisture, and the solvent. The maximum contribution from $Rh_6(CO)_{16}$, which exists at trace levels, was 0.5% of the total signal. Figure 8 shows that a characteristic reaction time is ca. 6.5 h.

Real Concentrations. Using the relative concentrations and knowing the initial moles of $Rh_4(CO)_9(\mu\text{-}CO)$ in each batch,

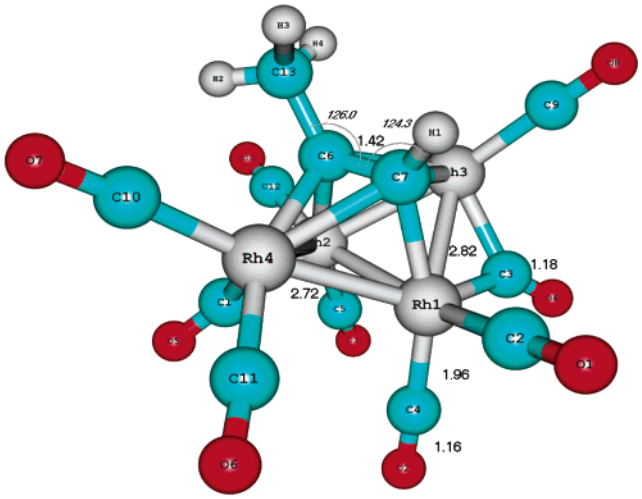

Figure 4. DFT-optimized geometry of μ_4-η^2-(1-propyne)$Rh_4(CO)_8$-(μ-CO)$_2$ using PBE/DGDZVP.

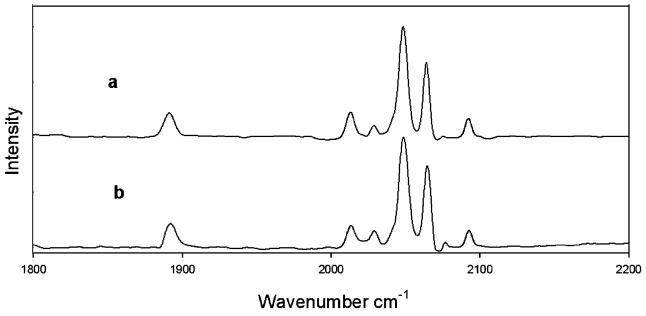

Figure 5. Low-resolution experimental spectra of (a) (μ_4-η^2-phenyl-1-hexyne)$Rh_4(CO)_8(\mu\text{-}CO)_2$ and (b) (μ_4-η^2-1-phenyl-1-butyne)Rh_4-$(CO)_8(\mu\text{-}CO)_2$.

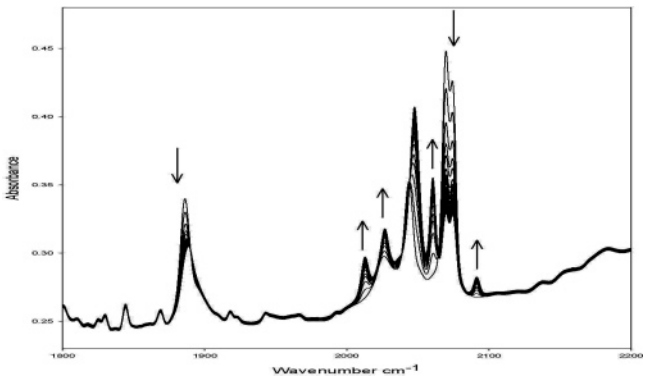

Figure 6. Time series of raw reaction spectra for the reaction of 3-hexyne with $Rh_4(CO)_9(\mu\text{-}CO)_3$.

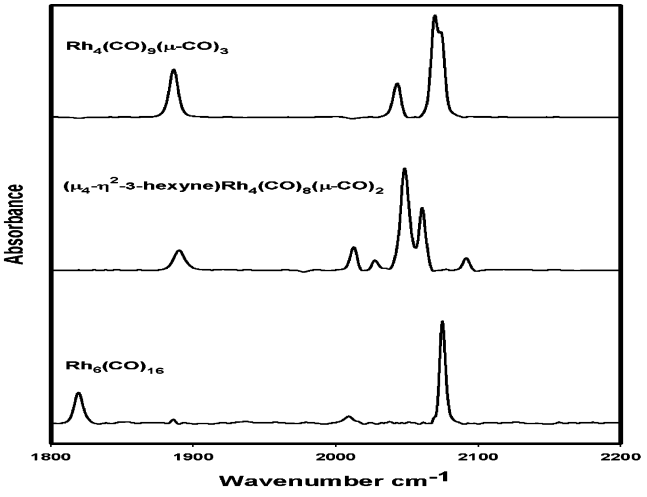

Figure 7. Pure component spectra obtained from BTEM analysis.

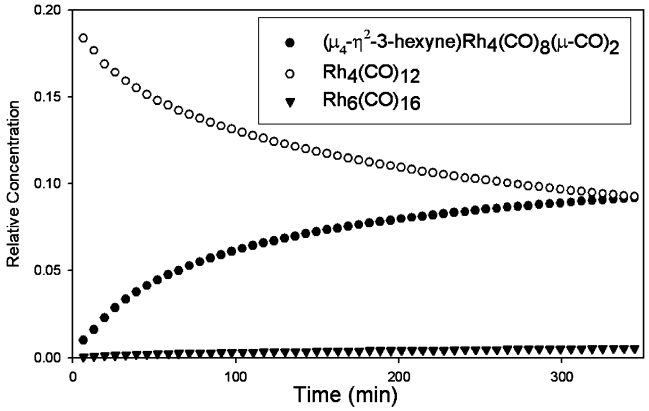

Figure 8. Relative metal carbonyl concentrations provided by BTEM analysis.

Table 3. Estimated Values of k_{obs} as a Function of Temperature

	temp (K)		
	288.15	293.15	298.15
k_{obs} (10^6 s^{-1})	1.4 ± 0.1	3.5 ± 0.2	8.1 ± 0.5

Table 4. Experimental Design for Kinetic Experiments

batch	experiment	$Rh_4(CO)_{12}$, mg	CO, bar	Ar bar	3-hexyne, μL	temperature, K
1	3-hexyne variation	40.60	0.03	0.988	3	298.15
2		40.60	0.03	0.988	4.5	298.15
3		39.60	0.03	0.988	6	298.15
4	$Rh_4(CO)_{12}$ variation	39.60	0.03	0.988	6	298.15
5		49.54	0.03	0.988	6	298.15
6		60.60	0.03	0.988	6	298.15
7	CO variation	40.15	0.01	1.008	6	298.15
8		39.60	0.03	0.988	6	298.15
9		39.56	0.05	0.968	6	298.15
10	temperature variation	40.76	0	1.018	6	288.15
11		39.39	0	1.018	6	293.15
12		40.42	0	1.018	6	298.15

the pure component can be scaled to the correct extension coefficient, and thus the real concentrations of all organometallics can be obtained. The arithmetic details are discussed in detail elsewhere.[30] Since quantitative information on 3-hexyne is not available in the 1800−2200 cm^{-1} spectral region, the time-dependent concentration of 3-hexyne was calculated using the mass balance shown below.

$$n_{\text{hexyne},t} = n_{\text{hexyne},t=0} - n_{\text{butterfly},t}$$

Kinetics and Mechanism of the Reaction. Nine kinetic experiments were performed to determine the rate expression for the formation of the butterfly cluster at 298 K. These experiments and can be divided into three sets, $Rh_4(CO)_{12}$ variation, 3-hexyne variation, and CO variation, as shown in Table 4 (see Experimental Section). In each set, one experimental parameter was systematically varied while the remaining variables were held essentially constant.

Figure 9 shows that the rate of formation of (μ_4-η^2-C_2H_5-CCC_2H_5)$Rh_4(CO)_8$(μ-CO)$_2$ increased with increasing $Rh_4(CO)_{12}$ and 3-hexyne. However, a drastic drop in the rate of its formation was observed when the CO mole fraction was increased, indicating that the coordination of the alkyne is poisoned/retarded by the presence of CO. The proposed mechanism, see Scheme 1, for the alkyne substitution reaction can

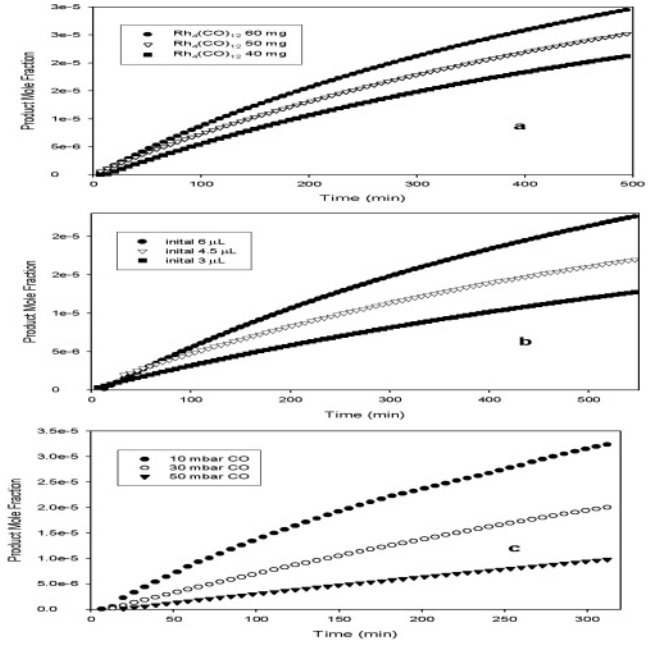

Figure 9. Mole fraction of (μ_4-η^2-$C_2H_5CCC_2H_5$)$Rh_4(CO)_8$(μ-CO)$_2$ as a function of reaction time: (a) $Rh_4(CO)_{12}$ variation, (b) 3-hexyne variation, and (c) CO partial pressure variation.

Scheme 1. Proposed Mechanism A for Eq 1 Which Involves the Dissociation of One of the Carbonyl Ligands from $Rh_4(CO)_9(\mu\text{-}CO)_3$ Prior to the Alkyne Attack

$$Rh_4(CO)_9(\mu\text{-}CO)_3 \underset{k_{-1}}{\overset{k_1}{\rightleftarrows}} Rh_4(CO)_{11} + CO \quad \text{(step 1)}$$

$$Rh_4(CO)_{11} + RC_2R \underset{k_{-2}}{\overset{k_2}{\rightleftarrows}} (RC_2R)Rh_4(CO)_{11} \quad \text{(step 2)}$$

$$(RC_2R)Rh_4(CO)_{11} \xrightarrow{k_3} (RC_2R)Rh_4(CO)_{10} + CO \quad \text{(step 3)}$$

be classified as a dissociative mechanism[31] where one of carbonyl ligands dissociates prior to the coordination of the ligand. DFT was performed, and the results suggest that apical CO dissociation may be preferred over basal (axial and radial) or bridging CO dissociation.

In Scheme 1, steps 1 and 2 are considered elementary. As step 3 is assumed to be the rate-limiting step, the rate of product formation can be presented as shown in eq 2.

$$\text{rate} = \frac{\mathrm{d}[(RC_2R)Rh_4(CO)_{10}]}{\mathrm{d}t} = k_3[(RC_2R)Rh_4(CO)_{11}] \quad (2)$$

As the intermediates $(RC_2R)Rh_4(CO)_{11}$ and $Rh_4(CO)_{11}$ were not observed, their accumulation can be assumed negligible, i.e., d[intermediate]/d$t \cong 0$. Using this steady-state approximation,[32] eq 2 can be rewritten as shown in eq 3.

$$\frac{\mathrm{d}[(RC_2R)Rh_4(CO)_{10}]}{\mathrm{d}t} = \frac{k_1[RC_2R][Rh_4(CO)_{12}]}{(k_{-1}/k_2)(1 + k_{-2}/k_3)[CO] + [RC_2R]} \quad (3)$$

With the assumption that k_3 is the rate-limiting step, the term k_{-2}/k_3 in the denominator is expected to be large, i.e., (k_{-1}/k_2)-$(1 + k_{-2}/k_3)[CO] \gg [RC_2R]$. Therefore, eq 3 can be further simplified as shown in eq 4, where k_{obs} equals $k_1/(k_{-1}/k_2)(1 + k_{-2}/k_3)$.

(29) Allian, A. D.; Garland, M. *J. Chem. Soc., Dalton Trans.* **2005**, *11*, 1957.
(30) Widjaja, E.; Li, C.; Garland, M. *J. Catal.* **2004**, *223*, 278.
(31) Richens, D. T. *Chem. Rev.* **2005**, *105*, 1961.
(32) Masel, R. I. *Chemical Kinetics and Catalysis*; John Wiley & Sons: New York, 2001.

$$\frac{d[(RC_2R)Rh_4(CO)_{10}]}{dt} = k_{obs}\frac{[RC_2R][Rh_4(CO)_{12}]}{[CO]} \quad (4)$$

To test eq 4, the orders of $Rh_4(CO)_9(\mu\text{-}CO)_3$, 3-hexyne, and CO were computed from the experimental data; that is, the values of α, β, and γ in eq 5 were obtained by fitting experimental concentration profiles using linear regression. The numerical values of α, β, and γ were 1.0362 ± 0.0199, 1.1061 ± 0.0232, and -1.0187 ± 0.0525, respectively.

$$\text{rate} = k_{obs}[Rh_4(CO)_{12}]^{\alpha}[\text{alkyne}]^{\beta}[CO]^{\gamma} \quad (5)$$

Although the results are in a good agreement with the suggested mechanism, it should be mentioned that the first step might instead involve transformation of the C_{3v} $Rh_4(CO)_9(\mu\text{-}CO)_3$ to another new structure, i.e., an open polyhedron, which results from the cleavage of one Rh−Rh metal bond. Indeed, there exist kinetic and mechanistic studies where open polyhedron M_4 clusters have been invoked in order to rationalize the observations.[33]

Apparent Eyring Activation Parameters. To determine the apparent activation parameters, four isothermal batch experiments were carried out at temperatures of 288.15, 293.15, and 298.15 K. The rate of the formation of $(\mu_4\text{-}\eta^2\text{-}C_2H_5CCC_2H_5)\text{-}Rh_4(CO)_8(\mu\text{-}CO)_2$ increased with increasing temperature. The observed rate constants, k_{obs}, are shown in the Table 3.

The values of k_{obs} were used to regress the values of the enthalpy of activation $\Delta H^{\ddagger}$ and the entropy of activation $\Delta S^{\ddagger}$ using eq 7. The obtained values were 123.6 ± 11.0 kJ·mol^{-1} and 72.4 ± 37.3 J·mol^{-1}·K^{-1}, respectively.

$$k_{obs} = \frac{\kappa T}{h}\exp\left(\frac{-\Delta H^{\ddagger}}{RT} + \frac{\Delta S^{\ddagger}}{R}\right) \quad (7)$$

Conclusion

The addition of alkyne to $Rh_4(CO)_{12}$ results in the formation of the butterfly clusters $(\mu_4\text{-}\eta^2\text{-alkyne})Rh_4(CO)_8(\mu\text{-}CO)_2$. The mid-infrared spectra of various butterfly clusters $(\mu_4\text{-}\eta^2\text{-alkyne})\text{-}Rh_4(CO)_8(\mu\text{-}CO)_2$ were obtained. Geometries for these new nonisolatable complexes were obtained by matching the experimentally obtained vibrational pattern in the mid-infrared with the predicted DFT vibrational patterns. The kinetics of the formation of the butterfly cluster $(\mu_4\text{-}\eta^2\text{-3-hexyne})Rh_4(CO)_8(\mu\text{-}CO)_2$ were also studied. The kinetics were well behaved and provided quite clear reaction orders. The experimental kinetics together with mechanistic considerations suggest that two different mechanisms are consistent with the observations. These involve, as a first step, either a CO dissociative mechanism or the cleavage of a Rh−Rh bond to form a coordinately unsaturated open polyhedron.

Experimental Section

General Information. All solution preparations were carried out under argon (Soxal, Singapore, 99.999%) using standard Schlenk techniques.[16] The solvents *n*-hexane (Fluka, puriss, 99.6%+) and d-benzene (Cambridge-Isotope, MA, 99.5%) were refluxed over sodium potassium alloy under argon. The argon was further purified prior to use by passage through a column containing 100 g of reduced BTS-catalyst (Fluka AG Buchs, Switzerland) and 100 g of 4 Å molecular sieves to adsorb traces of oxygen and water, respectively. The metal complex $Rh_4(CO)_{12}$ with stated purity of at least 98% was obtained from Strem Chemicals (Newport, MA). All alkynes, 3-hexyne, 1-heptyne,1-octyne, 4-octyne, 1-phenyl-1-hexyne, 1-phenyl-1-butyne (Aldrich, 99%), and the 1,6-enyne (GFS Chemicals, 99%) were used directly without further purification.

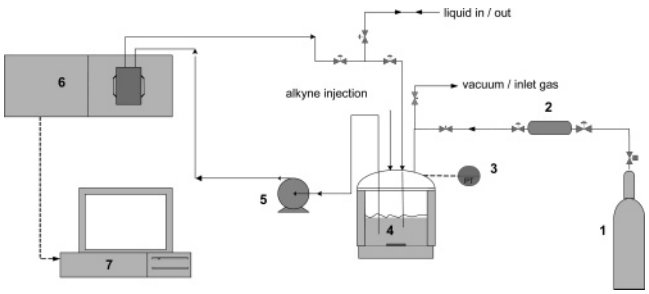

Figure 10. Experimental setup for in situ FTIR measurements. Legend: (1) argon tank; (2) argon purification column; (3) pressure transducer; (4) jacketed continuous stirrer tank reactor (CSTR); (5) hermetically sealed Teflon pump; (6) FTIR with high-pressure flow through cell; (7) data acquisition.

Equipment. All syntheses and kinetic runs were performed in a closed recycle system. The experimental apparatus consisted of a jacketed glass reactor (Aceglass) equipped with a magnetic stirrer, a Teflon membrane pump (Cole-Parmer), and a Perkin-Elmer System 2000 mid-infrared FTIR spectrometer. The fluid was pumped under isobaric (argon/CO, atmospheric pressure) and isothermal conditions (temp control Polyscience 9105, with temperature stability $\pm$ 0.05 K) from the reactor through the pump, then a high-pressure infrared cell with recycle back to reactor. Connections for vacuum and argon were provided. A 2.000 piezotransducer (PAA-27W, Keller AG, Switzerland) was used throughout for pressure measurements. The entire experimental setup was gastight. To ensure quantitative working conditions, and hence minimal decomposition of the moisture-, oxygen-, and light-sensitive metal complexes, the system was thoroughly rinsed with anhydrous solvent under argon and then evacuated to dryness prior to each experiment. In addition, the reactor was fully covered with aluminum foil, thus providing dark reaction conditions.[34]

Hamilton gastight 10 μL and 1.0 mL syringes were used for introducing 3-hexyne solutions into the reactor through a rubber septum. The high-pressure infrared cell was constructed at the ETH Zürich of SS316 steel and could be heated and cooled. The KBr single-crystal windows used (Korth Monokristalle, Kiel, Germany) had dimensions of diameter 40 mm by thickness 15 mm. Two sets of Viton and silicone gaskets provided sealing, and Teflon spacers were used between the windows. The construction of the flow-through cell is a variation on the design by Noack (1968)[35] and differs in some respects from other high-pressure infrared cells.[36] The high-pressure cell was situated in the Perkin-Elmer 2000 FTIR infrared spectrometer. The cell chamber was purged with purified nitrogen (Soxal, Singapore, 99.999%). The instrumental resolutions used were 1 and 4 cm^{-1}, and recorded spectra were obtained from 10 co-additions. The reported spectra from 1800−2200 cm^{-1} have 0.2 cm^{-1} data intervals. A schematic diagram of the experimental setup is shown in Figure 10.

Kinetic Experiments. The kinetic study consisted of 12 isothermal batch reactions. All of these batches were conducted in a similar manner. Thus, only a description of the first isothermal batch, conducted at 298.15 K and under 0.03 mbar CO, is provided in detail.

(33) Bor, G.; Dietler, U. K.; Pino, P. *J. Organomet. Chem.* **1978**, *154*, 301.

(34) Garland, M. In *Mechanisms in Homogeneous Catalysis: A Spectroscopic Approach*; Heaton, B., Ed.; Wiley-VCH: Weinheim, 2005; Chapter 4, p 157.

(35) Noack, K. *Spectrochim. Acta* **1968**, *24*, 1917.

(36) Whyman, R. In *Laboratory Methods in Vibrational Spectroscopy*, 3rd ed.; Willis, H. A., van der Maas, J. H., Miller, R. G., Eds.; Wiley: New York, 1987; Chapter 12.

Background spectra of the empty IR chamber were recorded, and only then was the high-pressure cell loaded into the IR compartment. Then, 40.60 mg of $Rh_4(CO)_{12}$ was added to 100 mL of distilled hexane in a Schlenk tube and stirred for 20 min under atmospheric argon. The reddish solution was then transferred to the evacuated reactor, the stirrer was started, and argon was introduced to a total pressure of 0.750 bar and allowed to equilibrate. Subsequently, 30 mbar of CO was carefully added to the reactor, and this was topped up with argon to 1.018 bar. The Teflon pump was started to allow fluid circulation through the high-pressure IR cell and back to the reactor. After equilibration of the entire system, infrared spectra of the $Rh_4(CO)_{12}$/*n*-hexane solution in the high-pressure cell were recorded. Reaction was initiated by injection of 6 μL of 3-hexyne dissolved in 1 mL of hexane through the rubber septum injection port. Directly after the injection, spectra were recorded every 5 min for ca. 14 h. The experimental design for all 12 experiments is shown in Table 4.

The solubility of CO in *n*-hexane was calculated using the Henry's constant reported in ref 37. Furthermore, due to the low CO partial pressures used, and the fact that CO is evolved during the reaction in eq 1, the partial pressure and mole fraction of dissolved CO had to be continuously updated as a function of extent of reaction. In this manner, proper kinetic analysis could be performed.

Attempts at Crystallization. Attempts to obtain crystals for X-ray single-crystal analysis have thus far been unsuccessful.

Spectral Processing. Band-target entropy minimization was used to obtain all the pure component experimental spectra reported in this contribution, by deconvolution of the corresponding reactive multicomponent solutions. Details of the mathematical constructs of BTEM can be found elsewhere.[26,27]

Single-batch experiments were performed to obtain the BTEM deconvolutions of the following pure component spectra in *n*-hexane: (μ_4-η^2-3-hexyne)$Rh_4(CO)_8$(μ-$CO)_2$ at 1 cm^{-1} resolution, (μ_4-η^2-1-heptyne)$Rh_4(CO)_8$(μ-$CO)_2$, (μ_4-η^2-phenylacetylene)Rh_4-$(CO)_8$(μ-$CO)_2$, (μ_4-η^2-1-phenyl-1-butyne)$Rh_4(CO)_8$(μ-$CO)_2$, and (μ_4-η^2-1-phenyl-1-hexyne)$Rh_4(CO)_8$(μ-$CO)_2$.

The pure component spectra of (μ_4-η^2-1-octyne)$Rh_4(CO)_8$(μ-$CO)_2$, (μ_4-η^2-4-octyne)$Rh_4(CO)_8$(μ-$CO)_2$, (μ_4-η^2-1-heptyne)Rh_4-$(CO)_8$(μ-$CO)_2$, and (μ_4-η^2-3-hexyne)$Rh_4(CO)_8$(μ-$CO)_2$ in d-benzene were obtained using the following procedure. Four batches of ca. 3 mg of $Rh_4(CO)_{12}$ dissolved in 0.5 mL of d-benzene were prepared. Then, an equimolar amount of alkyne was added to each batch, namely, 3-hexyne, 1-heptyne, 1-octyne, and 4-octyne. Upon injecting the respective alkyne to each $Rh_4(CO)_{12}$ solution, it was quickly transferred to a standard IR cell with a path length of 0.5 cm and was placed in the IR compartment to monitor the formation of the respective butterfly cluster. Undoubtedly, the inhomogeneity of the solution due to the lack of stirring contributed to the nonlinearity and the high noise level observed in the collected spectra. Nevertheless, BTEM was successfully able to reconstruct the pure component of the each formed butterfly cluster with decent signal-to-noise ratio and minor artifacts.

BTEM was applied to the kinetic batch experiments in order to get the following pure component spectra in *n*-hexane: (μ_4-η^2-3-hexyne)$Rh_4(CO)_8$(μ-$CO)_2$, $Rh_4(CO)_{12}$, and $Rh_6(CO)_{16}$.

DFT Calculations. Density functional theory was used to carry out full geometric optimization and vibrational assignments of (μ_4-η^2-2-butyne)$Rh_4(CO)_8$(μ-$CO)_2$ and (μ_4-η^2-1-propyne)$Rh_4(CO)_8$(μ-$CO)_2$. The PBEPBE density functional with the DGDZVP basis set was used, as this method successfully predicted the geometry and the vibrational spectra of a variety of rhodium carbonyl clusters.[38] DFT-predicted spectra in Figures 1 and 3 were presented in two formats. First is the direct output of the calculated vibrational spectra, while the second is plotted using Molden43, where Lorenzian distribution is used to represent the vibrational modes, which can be related easily to the experimental data.

To confirm the validity of the approach taken (functional and basis set used), the optimized geometry for (μ_4-η^2-HCCH)$Co_4(CO)_8$-(μ-$CO)_2$ and the mid-infrared spectra were predicted and compared to the available literature experimental results.[22] Very good agreement is obtained. These results are archived in the Supporting Information.

Acknowledgment. The authors wish to thank Prof. Mark Saeys for helpful discussions.

Note Added after ASAP Publication. In the version of this paper published on the Web March 21, 2006, two different equations were both labeled as eq 2. The version that now appears is correct.

Supporting Information Available: This material is available free of charge via the Internet at http://pubs.acs.org.

OM0510019

(37) Garland, M.; Horvath, I.; Bor, G.; Pino, P. *Organometallics* **1991**, *10*, 559.

(38) Allian, A. D.; Wang, Y.; Saeys, M.; Kuramshina, G. M.; Garland, M. *Vib. Spectrosc.*, in press.